Eigenstrain Techniques for Modeling Adaptive Structures: I) Active Stiffness Tailoring

ABDULMALIK A. A. ALGHAMDI[1,*] AND ABHIJIT DASGUPTA[2]

[1]*Department of Production Engineering and Mechanical Systems Design, King Abdulaziz University, Jeddah 21413, Saudi Arabia*

[2]*Department of Mechanical Engineering, University of Maryland, College Park, MD 20742, USA*

ABSTRACT: Three-dimensional eigenstrain techniques are used in this paper to model mechanical interactions in an active structure containing small embedded sensors and actuators. Eigenstrain techniques are used to predict the state of the strain inside the devices (sensors and actuators) under external and internal loads. The elastic energy of the structure is written in terms of the strain inside the devices, and an analytical dynamic model is developed based on a generalized form of Hamilton's variational principle. As an example, the dynamic response of an active cantilever beam containing embedded mini-devices is investigated analytically and experimentally. Specifically, active stiffness tailoring capabilities are explored. An analytical solution to the variational problem is obtained by using the Raleigh-Ritz approach. A numerical example is given and the response of the active structure is verified experimentally, using a cantilever beam made of Alplex plastic as host material and piezoelectric (PZT-5H) devices as active mini-devices for sensing and actuation. The analytical results show reasonable agreement with the experimental observations.

INTRODUCTION

Active materials and intelligent systems have attracted a great deal of interest from researchers for many years. Active structures have been used in the area of active vibration control by many researchers, see for example, Burke and Hubbard (1987), Tzou and Tseng (1990), Ha, Keilers and Chang (1992) and Reddy and Barbosa (2000). Piezoelectric materials have attracted significant attention for their potential application as sensors and actuators for controlling the response of active structures. In active structures, distributions of sensors, actuators, and data processing capability are used to modify, tune, and control the response of structures to sensed stimuli.

Numerous studies have modeled the interactions between devices and hosts in active structures. The response of active structures with assemblies of piezoelectric wafers in composite beams have been analyzed by using simple beam models (Bailey and Hubbard, 1985), pin force models (Crawley and de Luis, 1987), large deformation beam theory (Im and Atluri, 1989), laminate analysis (Crawley and Lazarus, 1991), nonlinear analysis (Pratt, Queine and Nayfah, 1999), and one-dimensional eigen-function approximations (Lin and Rogers, 1992). Variational methods have also been developed for solving the coupled boundary value problems in active structures. These include finite element methods (Allik and Hughes, 1970; Gaudenzi, 1997; Mahut, Agbosou and Pastor, 1998), Rayleigh Ritz methods (Hagood, Chung and Flotow, 1990) and strain energy methods (Wang and Rogers, 1991; Chee, Tong and Steven, 1998). In this paper, eigenstrain analysis is combined with a variational method as a modeling technique for active structures.

Most present-day active structural systems consist of relatively large surface-mounted "active" elements that can cause structural integrity problems due to high stress concentrations, poor interfacial bonding, change in the boundary conditions, etc. These limitations can be partially overcome by using mini-devices with less obtrusivity, and embedding them throughout the host to achieve adequate control authority. However, embedding of small devices produces three-dimensional stress interactions that are more difficult to model than those arising in surface-mounted devices and there is a lack of generic modeling techniques for such structures in the open literature. Nevertheless, number of devices increases by distributing them into the structure and this leads to less reliable system. The focus of this paper is one active structure with distributions of embedded devices whose volume fraction is less than 2%.

Eshelby's equivalent-inclusion technique (Eshelby, 1957) offers a convenient method to model the presence of an ellipsoidal heterogeneity inside an isotropic host structure. This technique is used in this paper to model the elastic interaction between actuators/sensors and the host, by using appropriate Green's functions. The equations of motion of the system are derived using a generalized Hamilton's principle. The resulting system is solved with a Rayleigh-Ritz technique. The change in the natural frequency of the structure due to harmonic excitation of the actuator is examined analytically.

*Author to whom correspondence should be addressed. E-mail: aljinaidi@hotmail.com

1045-389X/01/0? 0???-?? $10.00/0 DOI: 10.1106/42JH-8JG5-DNL8-XQT2
 Journal Online at http://techpub.metapress.com

Adaptivity of the beam is illustrated through active stiffening of the cantilever beam for position feedback control. Experimental verification of the analytical model is presented for a cantilevered Alplex beam containing small-embedded PZT-5H sensor/actuator mini-devices.

ANALYSIS

Eigenstrain is a name used in the literature (Mura, 1991) for stress-free strains such as unconstrained thermal expansion. A powerful and unified solution method, based on eigenstrain calculations, was introduced by Eshelby in the late fifties (Eshelby, 1957, 1959) to solve the elastic problem of an isotropic ellipsoidal heterogeneity inside an isotropic infinite matrix. Since then, this method has been used by many researchers for stress analysis in composite materials and fracture mechanics (Christensen, 1991; Mura, 1991).

As shown in Figure 1, an active structure with embedded mini-devices is modeled as a large elastic host medium with embedded ellipsoidal elastic heterogeneities. Host and device materials are approximated to be linear and mechanically isotropic.

The variational principle is a generalized form of Hamilton's principle, and may be written as (Tiersten, 1969),

$$\delta \int_{t_0}^{t} (L + W)\, dt = 0 \tag{1}$$

where δ is the variational operator, L is the Lagrangian functional; which is the difference between the kinetic energy and the electric enthalpy; W is the external work term, and (t_0, t) defines the time interval over which stationary values are sought.

The linear isothermal coupled electro-mechanical constitutive relation for piezoelectric material is given as (Ikeda, 1990),

$$\sigma_{ij} = \frac{\partial H}{\partial \varepsilon_{ij}} = C_{ijkl}\varepsilon_{kl} - e_{kij}E_k \tag{2}$$

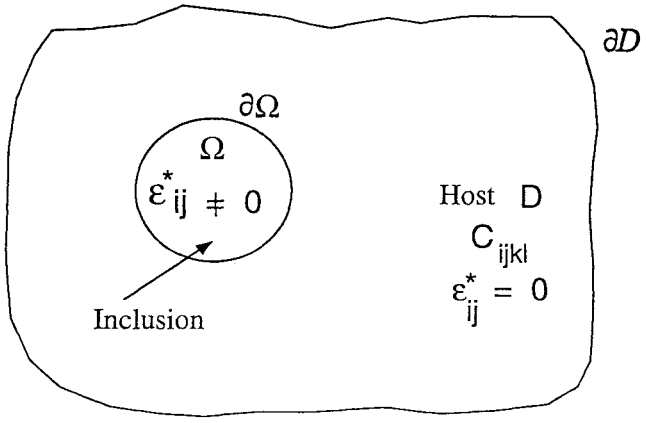

Figure 1. *Active structures.*

$$D_i = -\frac{\partial H}{\partial E_i} = e_{ikl}\varepsilon_{kl} + \varepsilon^{s}_{ij}E_j \tag{3}$$

where σ_{ij} is the stress tensor, H is the electric enthalpy, ε_{ij} is the strain tensor, C_{ijkl} is the mechanical stiffness tensor evaluated at constant (zero) electrical field, e_{ijk} is the piezoelectric stress coupling tensor, E_k is the electrical field vector, D_i is the electrical displacement vector, and ε^{s}_{ij} is the dielectric permittivity tensor evaluated at constant (zero) strain.

Using the definition of electric enthalpy (Tiersten, 1969), substituting for the work term (assuming only electrical work), and taking the first variation one can get,

$$\int_{t_0}^{t}\Big[\int_v \ddot{u}_i\rho\delta u_i dv + \int_v \varepsilon_{ij}C_{ijkl}\delta\varepsilon_{kl}dv - \int_\Omega \varepsilon_{ij}e_{kij}\delta E_k dv$$

$$-\int_\Omega \delta\varepsilon_{ij}e_{kij}E_k dv - \int_\Omega E_i\varepsilon^{s}_{ij}\delta E_j dv - \int_s Q\delta V dA\Big]dt = 0 \tag{4}$$

where u_i is the displacement vector, ρ is the density, v is the volume of the beam, Ω is the volume of the devices, Q is the specified surface charge density, V is the electric potential, and s is the electrode surface area of the devices. This is the electro-mechanical variational equation governing the active structure consisting of the host and the embedded devices. The integration domain in the above equation covers the host, sensors, and actuators. The structural effect of sensors and actuators on the structure is considered. If the direct piezoelectricity effect at sensors and actuators is ignored, then the electrical field is that due to potentials applied at the surface of the actuators.

In this paper, the eigenstrain technique is used to model the mechanical interactions in adaptive structures between embedded devices and the surrounding host structure. The eigenstrain technique provides a three-dimensional solution for mechanical interactions resulting from the presence of active (piezoceramics) elements. Also, the eigenstrain technique is capable of modeling the induced strains inside (piezoceramic) actuators caused by (electrical) excitation.

Consider an unbounded isotropic material with elastic constants C_{ijkl} containing a domain Ω (the heterogeneity) with elastic constants C^{d}_{ijkl} (see Figure 1). Assume that the heterogeneity has its own applied eigenstrains ε^{a}_{ij}. This applied eigenstrain is a result of the induced strain inside the inclusion ε^{a}_{ij}. Examples of ε^{a}_{ij} include thermo-mechanical, electro-mechanical, and magneto-mechanical strains.

Denote the applied strain at infinity by ε^{o}_{ij} and the disturbance strain, due to the presence of the heterogeneity and the applied eigenstrain, by ε'_{ij}. The disturbance stresses σ'_{ij} are in self-equilibrium, so that:

$$\sigma'_{ij,j} = 0 \tag{5}$$

The displacement boundary condition of the problem leads to:

$$u_i' = 0 \quad \text{at} \infty \tag{6}$$

Eshelby's method for modeling the disturbance field is based upon modeling the heterogeneity problem as an equivalent inclusion in homogenous media with fictitious eigenstrains ε_{ij}^f that produce the same stress field in Ω as the original heterogeneity.

The stress inside the heterogeneity is written using Hooke's law as,

$$\sigma_{ij} = \sigma_{ij}^o + \sigma_{ij}' = C_{ijkl}^d(\varepsilon_{kl}^o + \varepsilon_{kl}' - \varepsilon_{kl}^a) \quad \in \Omega \tag{7}$$

where

$$\sigma_{ij,j}^o = 0 \quad \in D \tag{8}$$

$$\sigma_{ij,j}' = 0 \quad \in D \tag{9}$$

$$u_i' = 0 \quad \in \partial D \tag{10}$$

Here ε_{ij}^a is the induced strain (produced by electrical excitation for electro-mechanical materials).

The heterogeneous inclusion is simulated by an inclusion in the homogenous material experiencing both an applied eigenstrain ε_{ij}^p, and an equivalent fictitious eigenstrain ε_{ij}^f,

$$\sigma_{ij} = \sigma_{ij}^o + \sigma_{ij}' = C_{ijkl}(\varepsilon_{kl}^o + \varepsilon_{kl}' - \varepsilon_{kl}^p - \varepsilon_{kl}^f) \quad \in \Omega \tag{11}$$

The fictitious eigenstrain ε_{ij}^f models mechanical interactions with the surrounding host structure due to external loads ε_{ij}^o, while the applied eigenstrain ε_{ij}^p models mechanical interactions resulting from the induced strain ε_{ij}^a. The equivalence between Equations (7) and (11) leads to (Mura, 1991)

$$C_{ijkl}^d(\varepsilon_{kl}^o + \varepsilon_{kl}' - \varepsilon_{kl}^a) = C_{ijkl}(\varepsilon_{kl}^o + \varepsilon_{kl}' - \varepsilon_{kl}^p - \varepsilon_{kl}^f) \tag{12}$$

If both the far-field strain ε_{ij}^o and the applied strain ε_{ij}^a are uniform, then the perturbations strain inside Ω is written as (Eshelby, 1957)

$$\varepsilon_{ij}' = S_{ijkl}(\varepsilon_{kl}^f + \varepsilon_{kl}^p) \equiv S_{ijkl}\varepsilon_{kl}^{**} \tag{13}$$

where the S_{ijkl} is Eshelby's fourth-order strain concentration tensor (see the Appendix) and total eigenstrain $\varepsilon_{ij}^{**} = \varepsilon_{ij}^p + \varepsilon_{ij}^f$.

To determine the total eigenstrain ε_{ij}^{**} one needs to substitute Equation (13) into Equation (12). The equivalence condition becomes,

$$C_{ijkl}^d(\varepsilon_{kl}^o + S_{klmn}\varepsilon_{mn}^{**} - \varepsilon_{kl}^a) = C_{ijkl}(\varepsilon_{kl}^o + S_{klmn}\varepsilon_{mn}^{**} - \varepsilon_{kl}^{**}) \tag{14}$$

Equation (14) represents a system of six linear independent equations for six independent components of the unknown eigenstrain tensor ε_{ij}^{**}.

In the absence of the induced strain ε_{ij}^a inside the heterogeneous inclusion, Equation (14) becomes,

$$C_{ijkl}^d(\varepsilon_{kl}^o + S_{klmn}\varepsilon_{mn}^{**}) = C_{ijkl}(\varepsilon_{kl}^o + S_{klmn}\varepsilon_{mn}^{**} - \varepsilon_{kl}^{**}) \tag{15}$$

where $\varepsilon_{ij}^{**} = \varepsilon_{ij}^f$.

This equation represents the heterogeneity problem (zero applied eigenstrain). One can solve for the fictitious eigenstrain ε_{ij}^f in terms of the far-field strain ε_{ij}^o as follows,

$$\varepsilon_{ij}^{**} = \varepsilon_{ij}^f = [(C_{ijkl}^d - C_{ijkl})S_{klmn} + C_{ijmn}]^{-1}(C_{mnpr} - C_{mnpr}^d)\varepsilon_{pr}^o \tag{16}$$

Similarly, for a heterogeneous inclusion in the absence of the applied far-field strain, Equation (14) becomes,

$$C_{ijkl}^d(S_{klmn}\varepsilon_{mn}^{**} + \varepsilon_{kl}^a) = C_{ijkl}(S_{klmn}\varepsilon_{mn}^{**} - \varepsilon_{kl}^{**}) \tag{17}$$

where $\varepsilon_{ij}^{**} = \varepsilon_{ij}^p$. The real eigenstrain ε_{ij}^p can be written in terms of the induced strain ε_{ij}^a in the heterogeneity as follows,

$$\varepsilon_{ij}^{**} = \varepsilon_{ij}^p[(C_{ijkl}^d - C_{ijkl})S_{klmn} + C_{ijmn}]^{-1}C_{mnpr}^d\varepsilon_{pr}^a \tag{18}$$

Thus, the total eigenstrain can be solved in terms of ε_{ij}^o and ε_{ij}^a.

Now by knowing the total eigenstrain, the perturbation strain inside the heterogeneity can be found using Equation (13) and the solution is complete.

The second term in Equation (4) can be written in terms of the eigenstrain as (Alghamdi and Dasgupta, 1993),

$$\begin{aligned}\int_V \varepsilon_{ij}C_{ijkl}\delta\varepsilon_{kl}dV &= \int_V \varepsilon_{ij}^o C_{ijkl}\delta\varepsilon_{kl}^o dV + \int_\Omega \varepsilon_{ij}^* C_{ijkl}S_{klmn}\delta\varepsilon_{mn}^* dV \\ &+ \int_\Omega \varepsilon_{ij}^o \Delta C_{ijkl}\delta\varepsilon_{kl}^o dV + \int_\Omega \varepsilon_{ij}^o \Delta C_{ijkl}S_{klmn}\delta\varepsilon_{mn}^* dV \\ &+ \int_\Omega \delta\varepsilon_{ij}^o \Delta C_{ijkl}S_{klmn}\varepsilon_{mn}^* dV + \int_\Omega S_{ijmn}\varepsilon_{mn}^* \Delta C_{ijkl}S_{klpr}\delta\varepsilon_{pr}^* dV\end{aligned} \tag{19}$$

where $\Delta C_{ijkl} = C_{ijkl}^d - C_{ijkl}$.

In the present analytical context, both sensors and actuators have a fictitious eigenstrain due to the external far-field loads, while the actuators have additional real eigenstrains due to the converse effect of the actuation voltage. As mentioned above, the real eigenstrains due to the direct effect at sensor and actuator are ignored because of their negligible magnitude in comparison to that associated with the converse effect due to the excitation voltage.

RAYLEIGH-RITZ APPROXIMATION

In this section the principle of dynamical modeling of adaptive structures are combined with eigenstrain techniques presented in the previous section for a one-dimensional adaptive structure in the form of adaptive beam. The analysis methodology for modeling mechanical interactions between the devices and the host using eigenstrain techniques, as presented in the previous section, is not limited to cantilever beams but can be used to model any structure by assuming appropriate strain distributions. Eigenstrain techniques are made to handle three dimensional structures, however, only one-dimensional beam problem is studied here in this paper to reduce complexity of algebraic manipulation and to illustrate the techniques in the first hand and to make it possible to be compared to an easy-to-make experimental setup.

The simple illustrative example chosen here is an active structure in the form of a cantilever beam with many embedded mini-devices. As shown schematically in Figure 2, two rows of uniformly spaced mini-devices are embedded in the beam symmetrically about the neutral plane of the beam. For simplicity, one row is assumed to contain all sensors, and the other all actuators. As the beam flexes, the outputs of individual sensors are used in a position-feedback circuit to actuate the corresponding (same *y*-location) active device (actuator) in the opposite row. The result is a stiffening of the beam and an accompanying increase in the natural frequency ω, if all losses in the system are ignored.

Assuming an Euler-Bernoulli beam formulation for the host cantilever, and in accordance with Rayleigh-Ritz techniques, the transverse displacement function (w) for the first vibrational mode is assumed to be sinusoidal in the *y*-*z* plane:

$$w = \left[1 - \cos\left(\frac{\pi y}{2l}\right)\right] r(t) \tag{20}$$

where l is the beam length, *y*-axis is oriented along the length of the beam, and $r(t)$ is a generalized mechanical degree-of-freedom representing the tip displacement. Equation (20) provides an approximate shape of the beam deflection. In more general situations, generic beam functions need to be used to approximate beam deflection. Also, due to the complexity of the eigenstrain techniques only the first mode of vibration is modeled here.

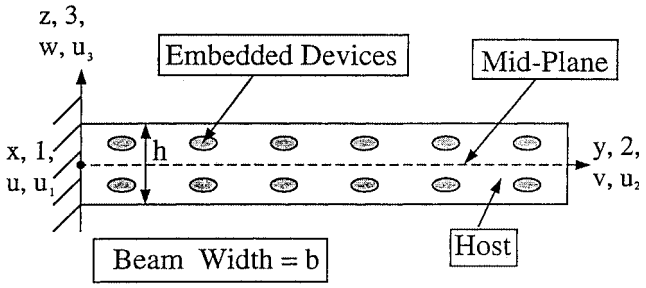

Figure 2. *The active cantilever beam.*

The voltage generated in the sensor is assumed to be proportional to the strain at that sensor (Alghamdi, 1995)

$$V_s = z_m \left(\frac{\pi^2}{4l^2}\right) \cos\left(\frac{\pi y_m}{2l}\right) h_{3ij} \theta_{ij} t_s r(t) \tag{21}$$

where z_m and y_m are the coordinate of the mid point of the sensor, h_{3ij} is the piezoelectric voltage-strain coupling tensor, θ_{ij} is the constant solution tensor defined as,

$$\theta_{ij}(\vec{x}) = \gamma_{ij}(\vec{x}) + S_{ijkl}\eta_{kl}(\vec{x}) \tag{22}$$

where γ_{ij} is the appropriate shape function for the strain field in the beam, and η_{ij} is defined as,

$$\eta_{ij}(\vec{x}) = [(C^d_{ijkl} - C_{ijkl})S_{klmn} + C_{ijmn}]^{-1}(C_{mnpr} - C^d_{mnpr})\gamma_{kl}(\vec{x}) \tag{23}$$

and t_s is the sensor thickness.

The electrical voltage applied at the surface of the actuator is proportional to the sensor voltage (V_s)

$$V = GV_s \tag{24}$$

where G is the constant feedback gain. Substituting Equations (13), (16) and (19) into Equation (4) and allowing arbitrary variation of $r(t)$ and $V(t)$, one obtains the following set of equations for the system,

$$M\ddot{r}(t) = C_p\dot{r}(t) + K_p r(t) + K_a V(t) = 0 \tag{25}$$

$$K_a r(t) + S_a V(t) = q \tag{26}$$

where M, K_p, C_p K_a, and S_a are the mass, stiffness, passive structural damping, electro-mechanical coupling, and capacitance, respectively, and q is the applied charge at the surfaces of the actuators. The passive stiffness term (K_p), the active stiffness term (K_a) and the electrical term (S_a) were all calculated using eigenstrain analysis developed in the previous section. Details of these terms can be found in Alghamdi (1995).

The type of structure under investigation, see Figure 2, has discrete actuators of simple geometry where the potential fields are assumed directly and measured experimentally. The value of $V(t)$ in Equation (25) ("actuator" equation) is calculated using Equations (21) and (24). Equation (26) ("sensor" equation) relates the applied voltage and the mechanical displacement to the surface charges.

Substituting Equations (21) and (24) in (25),

$$M\ddot{r}(t) + C_p\dot{r}(t) + [K_p + K_a G^T]r(t) = 0 \tag{27}$$

where G_T is the total feedback gain representing feedback

gain (G) and the appropriate piezoelectric coupling coefficient.

For harmonic motion, the square of the first frequency of the system is

$$\omega_1^2 = \frac{K_p + G^T K_a}{M} \tag{28}$$

The frequency response function is

$$\alpha = \frac{1}{\sqrt{(K_p + G^T K_a - \omega^2 M)^2 + (\omega C_p)^2}} \tag{29}$$

where ω is the excitation frequency.

ANALYTICAL RESULTS

The primary focus of this paper is to develop a technique to analyze active structures that have many small active elements instead of a few large ones. The goal of this simple dynamic analysis is to show the capability of eigenstrain techniques to model responses of active structures, in particular active stiffening. Experimental verification of these results is presented in the following section.

The chosen beam in this study has the dimensions shown in Figure 3. Device volume-fraction (V_f) is kept at 2% in the theoretical analysis to minimize the mechanical interactions between the devices. The change in the first frequency of the structure due to harmonic excitation along with a shift in the peaks of the frequency response functions (FRF) of the damped system are presented as measures of active stiffening.

The "actuator" equation is written in terms of the fundamental frequency ω, as given by Equation (28), and in terms of the magnitude of the frequency response function as given by Equation (29).

Effect of Device Density

Figure 4 shows the effect of increasing the size of the device (hence device volume-fraction) on active stiffening, at four device pairs (n = 4). The maximum device volume-fraction (V_f) is only 2% of the beam volume. Feedback gain (G) is increased from 0 to 38.

Results presented in Figure 4 illustrate the increase in the active stiffening as feedback gain increases for V_f = 0.5, 1.1, and 2%. The fundamental frequency is normalized with respect to the frequency for n = 4 and the corresponding device volume-fraction at zero feedback gain (G = 0). As expected, active stiffening (represented by the change in the normalized system frequency) increases as the device volume-fraction increases. More than a 4% change in the first natural frequency is achieved for n = 4 and V_f = 2% at G = 38 and the corresponding electrical field at the actuator near the fixed end (E_{max}) is 1000 V/mm.

Effect of Host Stiffness

Figure 5 illustrates the dependence of the fundamental frequency, and hence the active stiffening effect, on the Young's modulus of the host material for different feedback gains. The fundamental frequency is normalized with respect to that of the passive beam at zero feedback gain, and the host stiffness is varied from that of Alplex to that of aluminum.

The active stiffening effect rises sharply and then decreases with increasing host stiffness. This means that there is an optimum value for the host stiffness to maximize active stiffening. To understand the reason for this optimal host stiffness, consider qualitatively, the host-actuator interactions. When the host is very compliant, the strain caused by the actuator does not cause a large change in the strain energy (and hence system frequency). As an extreme example, the actuator strain would obviously have no effect if the host has zero stiffness (air). Conversely, when the host is very stiff, the

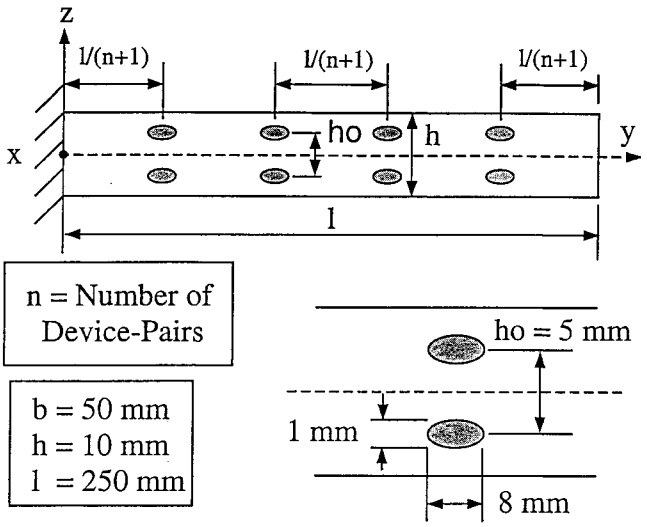

Figure 3. *Dimensions of the modeled active cantilever beam.*

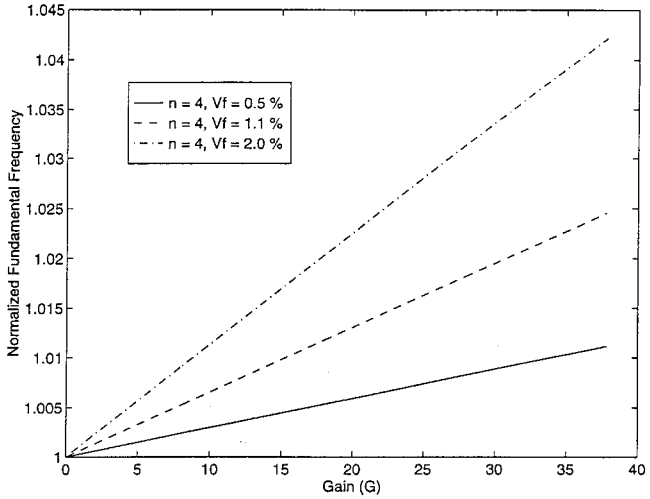

Figure 4. *Effect of increasing device density on active stiffening.*

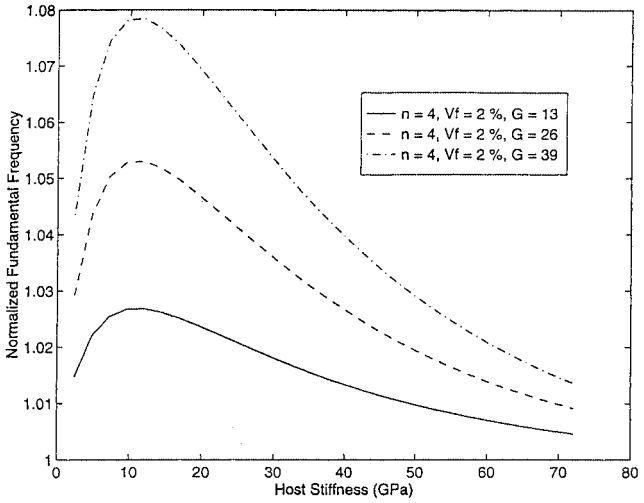

Figure 5. *Effect of host stiffness on active stiffening.*

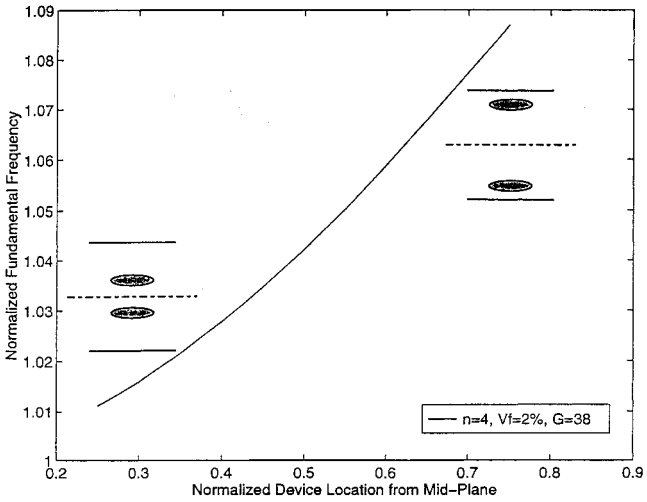

Figure 7. *Effect of changing device location on active stiffening.*

actuator lacks the authority to produce large perturbations in the host strain field or host strain energy. Thus, stiffening effect decreases in very stiff hosts. The optimum stiffening effect is therefore encountered in hosts of some intermediate stiffness. The actual stiffness at which this optimum stiffening effect occurs, is dependent on system parameters such as actuator stiffness, actuator voltage, beam geometry, boundary conditions, actuator volume fraction, etc. That optimum value for this structure occurs at host stiffness equal to 12 GPa, which is about 20% of the PZT device stiffness. Therefore, choosing the proper host and device stiffnesses can maximize active stiffening. Similar optimization can also be achieved through the use of coatings of appropriate stiffness.

Effect of Feedback Gain

Figure 6 demonstrates the effect of changing feedback gain, on the FRF of the active beam. The plot shows active stiffening by shifting to a higher frequency due to the increase in the feedback gain (G) from zero to 38 at $n = 4$ and $V_f = 2\%$. The first natural frequency of the beam at zero feedback gain is 43.41 Hz. This value increases to 44.34 Hz and 45.24 Hz at $G = 19$ and 38, respectively. The percentage increase in the first natural frequency at $G = 38$ is 4.2%, as depicted in Figure 4.

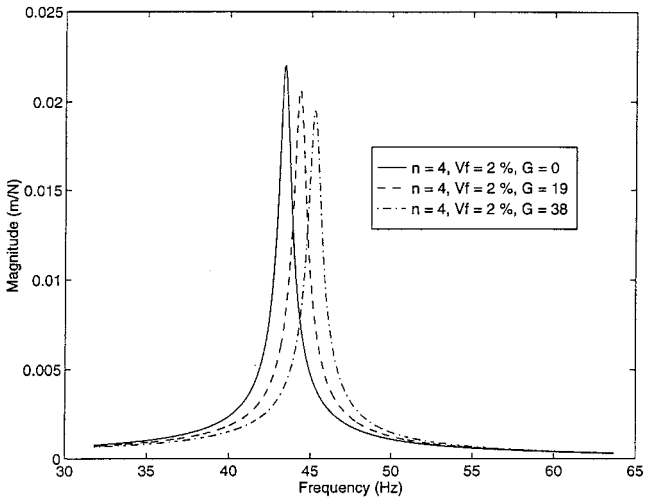

Figure 6. *Effect of feedback gain on active stiffening (FRF).*

Effect of Device Location

Figure 7 shows the change in the active stiffening effect as a function of device location relative to the beam mid-plane. Feedback gain, number of device-pairs, and device density are all held constant. The fundamental frequency is normalized with respect to that of the passive beam ($G = 0$) with the appropriate device location. Device location is normalized with respect to half of the beam thickness. Normalized device location (l_o) of 0.5 corresponds to devices located half the distance between beam mid-plane and free surface. As the devices move away from the mid-plane, sensors and actuators achieve more sensitivity and authority, respectively. However, the electrical field is directly proportional to the distance from the beam mid-plane, and one should consider its value for constant feedback gain to avoid any depoling of the piezoceramic actuators.

Devices at $l_o = 0.25$ are able to stiffen the beam by only 1.1% at $E_{\max} = 500$ V/mm, while devices located half the way from beam mid-plane ($l_o = 0.5$) produce 4.2% active stiffening at $E_{\max} = 1000$ V/mm. At $l_o = 0.75$ the beam stiffens by 8.7% at $E_{\max} = 1500$ V/mm.

EXPERIMENTAL VERIFICATION

An active cantilever beam was fabricated in the Smart Materials and Structures Research Center (SMSRC) at the University of Maryland, College Park. As shown in Figure 8, the beam width is 25.4 mm, the length is 203.2 mm, and the thickness is 3.6 mm. The piezoelectric device thickness (in z-direction) is 0.25 mm, the length (in y-direction) is 6.4 mm, and the width (in x-direction) is 25.4 mm. Device location

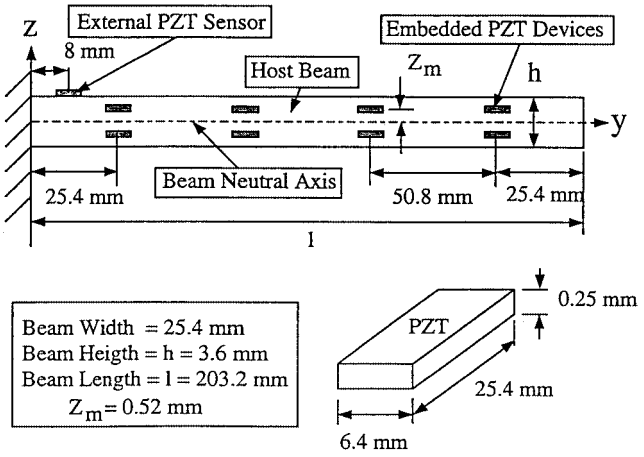

Figure 8. *Dimensions of the fabricated active beam.*

Table 2. Material properties of piezoceramic (PZT-5H).

Dielectric permittivity, ε_{33}^T	301 (10^{-10} F/m)
ε_{33}^S	130 (10^{-10} F/m)
ε_{11}^T	277 (10^{-10} F/m)
ε_{11}^S	151 (10^{-10} F/m)
Piezielectric strain coupling, d_{31}	–274 (10^{-12} m/V)
d_{33}	593 (10^{-12} m/V)
d_{15}	741 (10^{-12} m/V)
Elastic compliance (@ constant *E*), S_{11}^E	16.5 (10^{-12} m^2/N)
S_{33}^E	20.7 (10^{-12} m^2/N)
S_{44}^E	43.5 (10^{-12} m^2/N)
S_{12}^E	–4.78(10^{-12} m^2/N)
S_{13}^E	–8.45 (10^{-12} m^2/N)
Density	7500 (Kg/m^3)

(l_o) is 0.29. Material properties of the host and the PZT devices are given in Tables 1 and 2.

The experimental study of the active structure presented in this research is different from most of the published articles (Bailey and Hubbard, 1985; Crawley and de Luis, 1987; Hagood, Flotow and Von, 1991). This is because sensors and actuators are relatively small in comparison to devices used by other researchers. Dimensions of the piezoelectric elements are at least one order of magnitude less than the dimensions of the cantilever beam in *y-z* plane, as shown in Figure 8. As mentioned before, the reason for choosing small devices is to reduce the obtrusivity and hence promote better structural integrity of the device.

The first two pairs of devices (a pair denotes a sensor and the corresponding actuator on the opposite side of the beam neutral axis, as shown in Figure 2) from the fixed end are used for active vibration control. The third pair is used to excite the beam during forced vibration tests. The amount of strain (or voltage output) measured at the fourth pair is too small for the cantilever configuration. Therefore, devices of the fourth pair are not used in this setup. Nevertheless, this pair could be useful if the active beam is used in other configurations like simply supported or fixed-fixed boundary conditions.

An external piezoceramic element having the same dimensions as the embedded devices is bonded to the external surface of the beam 8 mm from the fixed end of the beam, as shown in Figure 8. This PZT is used as a general sensor because interactions between stress fields of sensor and actuator are ignored in the developed model.

The feedback system is shown in Figure 9 for the frequency response test. It consists of voltage pre-amplifier connected to the external PZT sensor. The pre-amplifier is connected to a 3202 Krohn-Hite low-pass frequency filter to filter out noises generated in the system.

The signal coming out of the frequency filter is sent to two different circuits leading to the actuators of the first and the second device-pairs. Each loop is designed to condition the signal before it goes to the actuator of the proper device-pair. The frequency filter is connected to two different phase shifters. The phase shifter is used to adjust the phase between sensor output voltage and the voltage sent to the actuator. The phase shifter is adjusted manually at excitation frequency equal to the first natural frequency of the beam. A Crown Comp-Tech 400 power amplifier is connected to the phase shifter to amplify the signal before it goes to each actuator.

The experimental value of the feedback gain in each sensor-actuator circuit is computed as the ratio between the actuator voltage V_a and the sensor voltage V_s (see Figure 9). The alternate value of the sensor voltage is estimated from the external sensor as follows,

Table 1. Material properties of the host.

Modulus of elasticity	2.4 (GPa)
Poisson's ratio	0.3
Density	1200 (Kg/m^3)

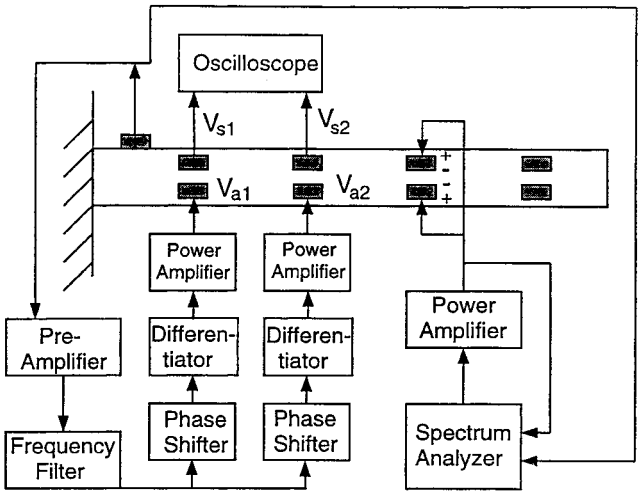

Figure 9. *Experimental setup.*

$$V_s = \frac{V_{so}}{V_{eo}} V_e \tag{30}$$

where V_{so} is the sensor output in the passive beam (at zero feedback gain), V_{eo} is the corresponding output of the external sensor (at zero feedback gain), and V_e is the instantaneous output of the external sensor. Thus, (V_{so}/V_{eo}) is the empirical calibration factor used to estimate the output of the embedded sensors from the external sensor. The reason for this approximated approach is due to the limitation in the theoretical model in accounting for the interactions between sensor and actuator.

In forced vibration tests, a sweep sinusoidal voltage of amplitude of 5 V is generated using a Spectrum Analyzer (HP 35665A). This signal is amplified to 120 V signal using a power amplifier (Crown Comp-Tech 400), and applied to the third pair. The two devices of the third pair are driven 180° out-of-phase in order to drive the beam in pure bending.

The frequency response is measured using the Spectrum Analyzer which compares the voltage input to the devices of the third pair, with the output voltage measured at the external attached PZT sensor, as shown in Figure 9. Experimental frequency response data is recorded by the digital Spectrum Analyzer and then downloaded to a computer for analysis and post-processing.

Time response is measured by connecting the external PZT to an oscilloscope. The tip of the beam is given some fixed initial displacement (r_o) and the beam is allowed to vibrate under active vibration control. The time response of the active beam is captured by an oscilloscope (Nicolet 320 Digital Oscilloscope).

In active stiffening, the electrical field applied to the actuator is proportional to the sensor voltage. The electrical field supplied to each actuator is 180° phase shifted with respect to the electrical field generated by the sensor of that pair. In principle, it is possible to use sensors of the first two pairs as additional actuators. However, because of mechanical interaction effects, only one device of each pair is used as an actuator. Since the model does not account for the mechanical interactions between opposite devices in each pair, using them simultaneously as actuators would make it difficult to compare experimental results with analytical predictions.

Additional reasons for deviations between experimental results and analytical predictions are the assumptions made in the model such as: perfect interfacial bonding condition is assumed in the model, the rectangular cross-section of the devices is approximated to be elliptical with equivalent areas in the analytical model, the electrical losses in the system are ignored in the model, the finite dimensions of the host in the z direction are considered very approximately in the eigenstrain analysis, mechanical interactions between the embedded devices are ignored in the model, the sensor outputs are estimated in the experiment from the external PZT sensor, and the nonlinearities in the material properties of the devices have been ignored. Because of the difficulties in accounting for these approximations explicitly, a scalar calibration coefficient (k) is assumed in the model to simulate the effects of the above simplifications in the model. One can estimate the value of the coefficient based on some simple experimentation. The beam is given a known tip displacement and the voltage output of an embedded sensor is recorded. Sensor voltage output is compared with the analytical prediction. The experimental value is 0.75 of the analytical prediction. This implies 25% loss at the sensor; in other words, the sensor calibration coefficient (k) is 0.75. Or the overall electro-mechanical efficiency of the embedded devices is 75% in the static case.

Figure 10 shows a comparison between the experimental and the analytical results. The x-axis is the feedback gain (G) whereas the vertical axis is the normalized fundamental frequency. The fundamental frequency is normalized with respect to that of the passive beam ($G = 0$). Experimental values of the first frequency are obtained using frequency response tests. Note that experimental results for one ($m = 1$) and two ($m = 2$) active pairs have the same trend as the analytical prediction.

The calibration factor (k) in the model represents the losses in energy transformation at the sensors and actuators. In other words, the electrical energy generated at sensors due to the direct effect is only 75% of the total available from the applied mechanical energy. On the other hand, only 75% of the total mechanical energy available from the applied electrical energy at actuators is transferred to the host by the converse effect. Therefore, since sensors and actuators have the same working environment, their "efficiency" is assumed to be 75%. Figure 10 shows comparisons between experimental results and model predictions, assuming "losses" of 25%.

The comparison between the experimental results and model predictions in time domain is given in Figure 11. The y-axis is the normalized external sensor output measured ex-

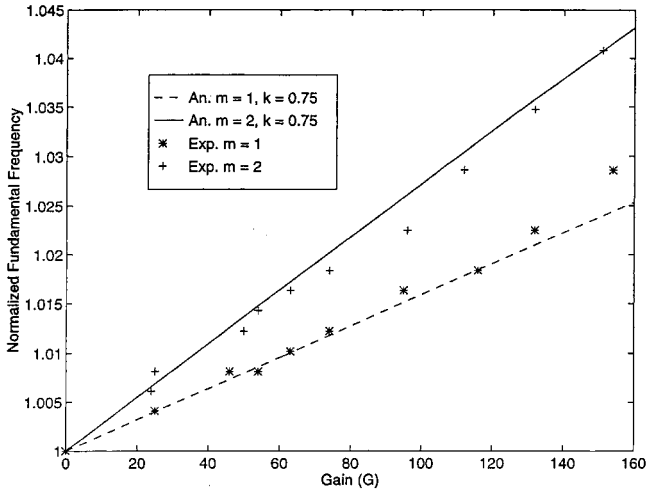

Figure 10. *Comparison between analytical and experimental active stiffening, assuming losses in the system.*

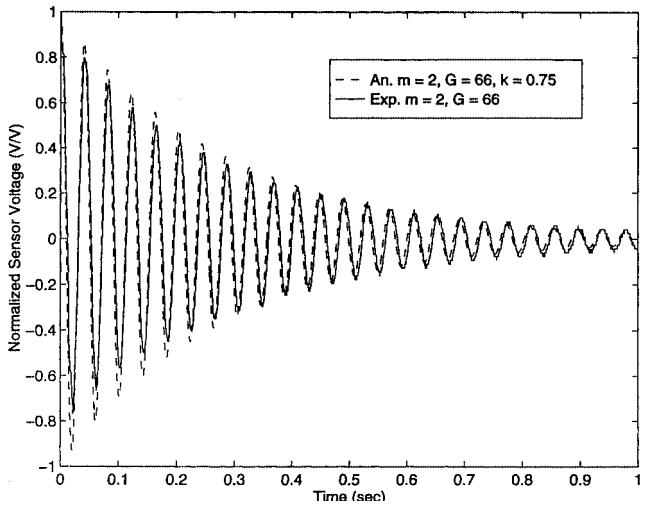

Figure 11. *Comparison between analytical and experimental active stiffening in time domain for two active pairs.*

perimentally or predicted analytically. The solid line represents the experimental response of the beam, whereas the dashed line gives the analytical response of the beam. The response is given for two active pairs ($m = 2$) at $G = 66$. Again, the ability to achieve good agreement between experimentally measured and analytically predicted response with use of only one fixed scalar calibration factor ($k = 0.75$), illustrates the ability of the eigenstrain method to represent the basic mechanics of the active structure with embedded mini-devices.

It is worth mentioning in closing that the small change in the dynamic response is due to the small volume fraction of the devices, which is only 0.22% for each actuator.

CONCLUSIONS

Analytical predictions based on Hamilton's principle are compared with experimental data for active stiffening of a cantilever beam with embedded mini-actuators. The mechanical interactions between the host and the devices are modeled using an eigenstrain method. Active stiffening of the active beam was achieved experimentally by using constant-gain position-feedback control. This paper demonstrates the ability of eigenstrain methods to successfully model active structures containing mini-devices.

ACKNOWLEDGEMENTS

This work has been partially supported by the Army Research Office under their University Research Initiative. The program monitor is Gary Anderson.

APPENDIX

Eshelby's fourth-order concentration tensor S_{ijkl} for uniform field is given as,

$$S_{ijkl}(\lambda) = \frac{1}{8\pi(1-\nu)}\delta_{ij}\delta_{kl}[2\nu I_i(\lambda) - I_k(\lambda) + ai^2 I_{kl}(\lambda)]$$

$$+ (\delta_{ik}\delta_{jl} + \delta_{jk}\delta_{il})[ai^2 I_{ij}(\lambda) - I_j + (1-\nu)[I_k(\lambda) + I_l(\lambda)]] \tag{A1}$$

where ν is Poisson' ratio of the matrix, δ_{ij} is Kronecker delta, ai are the semi axes of the ellipsoid inclusion. Integrals I_i and I_{ij} are defined as follow:

$$I_i(\lambda) = 2\pi a1a2a3\int_\lambda^\infty \frac{ds}{(ai^2+s)\Delta(s)} \tag{A2}$$

$$I_{ij}(\lambda) = 2\pi a1a2a3\int_\lambda^\infty \frac{ds}{(ai^2+s)(aj^2+s)\Delta(s)} \tag{A3}$$

where $\Delta(s)$ is defined as,

$$\Delta(s) = \sqrt{(a_1^1+s)(a_2^2+s)(a_3^2+s)} \tag{A4}$$

and λ is the largest positive root of

$$\frac{x_i x_i}{ai^2+\lambda} = 1 \tag{A5}$$

for exterior points (in the host), and $\lambda = 0$ for interior points (inside inclusion). The above *I*-integrals can be expressed in terms of standard elliptic integrals (Moschovidis, 1975).

REFERENCES

Alghamdi, A. A. 1995. "Response of Active Structures with Multiple Embedded Devices Using Eigenstrain Techniques," Ph. D. Thesis, University of Maryland, College Park.

Alghamdi, A. A. and Dasgupta, A. 1993. "Micromechanical Dynamic Analysis of an Active Beam with Embedded Distributions of Piezoelectric Actuator/sensor Devices," *Active Structures and Material Systems, The 1993 ASME Winter Annual Meeting,* AD-Vol. 35, New Orleans, Louisiana, pp. 121–128.

Allik, H. and Hughes, T. J. R. 1970. "Finite Element Method for Piezoelectric Vibration," *International Journal for Numerical Methods in Engineering,* 2:151–157.

Bailey, T. and Hubbard, J. E. Jr. 1985. "Distributed Piezoelectric-Polymer Active Vibration Control of a Cantilever Beam," *AIAA Journal of Guidance, Control and Dynamics,* 8(5):605–611.

Burke, S. E. and Hubbard, J. E. Jr. 1987. "Active Vibration Control of a Simply Supported Beam Using a Spatially Distributed Actuator," *IEEE Control Systems Magazine,* 7(6):25–30.

Chee, C. Y. K. et al. 1998. "A Review on the Modelling of Piezoelectric Sensors and Actuators Incorporated in Intelligent Structures," *Journal of Intelligent Material Systems and Structures,* 9(9):3–19.

Christensen, R. M. 1991. *Mechanics of Composite Materials,* Krieger Publishing Company, Malabar, Florida.

Crawley, E. F. and de Luis, J. 1987. "Use of Piezoelectric Actuators as Elements of Intelligent Structures," *AIAA Journal,* 25(10):1373–1385.

Crawley, E. F. and Lazarus, K. B. 1991. "Induced Strain Actuation of Isotropic and Anisotropic Plates," *AIAA Journal,* 29(6):944–951.

Dasgupta, A. and Alghamdi, A. A. A. 1992. "Interaction Mechanics Between Embedded Micro-Actuators and the Surrounding Host in Smart Structures," *Proceedings of the American Society for Composites, Seventh Technical Conference*, University Park, Pennsylvania, pp. 919–928.

Eshelby, J. D. 1957. "The Determination of the Elastic Field of an Ellipsoidal Inclusion and Related Problems," *Proceedings of the Royal Society*, Series A, 241:376–396.

Eshelby, J. D. 1959. "The Elastic Field Outside an Ellipsoidal Inclusion," *Proceedings of the Royal Society*, Series A, 252:561–569.

Gaudenzi, P. 1997. "On the Electromechanical Response of Active Composite Materials with Piezoelectric Inclusions," *Computers & Structures*, 65 (2):157–168.

Ha, S. K. et al. 1992. "Finite Element Analysis of Composite Structures Containing Distributed Piezoceramics Sensors and Actuators," *AIAA Journal*, 30(3):772–780.

Hagood, N. W. et al. 1990. "Modeling of Piezoelectric Actuator Dynamics for Active Structural Control," *Journal of Intelligent Material Systems and Structures*, 1(3):327–354.

Hagood, N. W. et al. 1991. "Damping of Structural Vibrations with Piezoelectric Materials and Passive Electric Networks," *Journal of Sound & Vibration*, 146(2):243–268.

Ikeda, T. 1990. *Fundamentals of Piezoelectricity*, Oxford Science Publications, Oxford.

Im, S. and Atluri, S. N. 1989. "Effects of a Piezo-Actuator on a Finitely Deformed Beam Subjected to General Loading," *AIAA Journal*, 27(12):1801–1807.

Lin, M. W. and Rogers, C. A. 1992. "Analysis of a Beam Structure with Induced Strain Actuators Based on an Approximated Linear Shear Stress Field," *Proceedings of the Recent Advances in Active and Sensory Materials and Their Applications*, Blacksburg, Virginia, pp. 363–376.

Mahut, T. et al. 1998. "Dynamic Analysis of Piezoelectric Fiber Composite in an Active Beam Using Homogenization and Finite Element Methods," *Journal of Intelligent Material Systems and Structures*, 9(12):1009–1017.

Moschovidis, Z. A. 1975. "Two Ellipsoidal Inhomogeneities and Related Problems Treated by the Equivalent Inclusion Method," Ph.D. Dissertation, Northern University, Evanston, Illinois.

Mura, T., 1991. *Micromechanics of Defects in Solids*, 2ed Revised Edition, Kluwer Academic Publishing, Boston.

Pratt, J. R. et al. 1999. "Terfenol-D Nonlinear Vibration Absorber," *Journal of Intelligent Material Systems and Structures*, 10(1):38–58.

Reddy, N. J. and Barbosa, J. I. 2000. "On Vibration Suppression of Magnetostrictive Beams," *Journal of Smart Materials and Structures*, 9(1):49–58.

Tiersten, H. F., 1967. "Hamilton's Principle for Linear Piezoelectric Media," *Proceedings Letters, Proceedings of the IEEE*, pp. 1523–1524.

Tiersten, H. F. 1969. *Linear Piezoelectric Plate Vibrations*, Plenum Press, New York.

Tzou, H. S., 1993. *Piezoelectric Shells: Distributed Sensing and Control of Continua*, Kluwer Academic Publishers, Boston.

Wang, B-T and Rogers, C. A. 1991. "Modeling of Finite-Length Spatially-Distributed Induced Strain Actuators for Laminated Beams and Plates," *Journal of Intelligent Material Systems and Structures*, 2(1):38–58.